PCCP

Accepted Manuscript

This is an *Accepted Manuscript*, which has been through the Royal Society of Chemistry peer review process and has been accepted for publication.

Accepted Manuscripts are published online shortly after acceptance, before technical editing, formatting and proof reading. Using this free service, authors can make their results available to the community, in citable form, before we publish the edited article. We will replace this *Accepted Manuscript* with the edited and formatted *Advance Article* as soon as it is available.

You can find more information about *Accepted Manuscripts* in the Information for Authors.

Please note that technical editing may introduce minor changes to the text and/or graphics, which may alter content. The journal's standard Terms & Conditions and the Ethical guidelines still apply. In no event shall the Royal Society of Chemistry be held responsible for any errors or omissions in this *Accepted Manuscript* or any consequences arising from the use of any information it contains.

ROYAL SOCIETY OF CHEMISTRY

www.rsc.org/pccp

Please do not adjust margins

Journal Name

ARTICLE

Interaction of iron with a wagon wheel ultrathin TiO_x film grown on Pt(111)

Received 00th January 20xx,
Accepted 00th January 20xx

DOI: 10.1039/x0xx00000x

www.rsc.org/

Luca Artiglia,*[a] Emanuele Cavaliere,[b] Luca Gavioli,[b] Gian Andrea Rizzi[a]

The structure and thermal evolution of Fe nanoparticles deposited on a wetting TiO_x ultrathin film epitaxially grown on Pt(111) has been characterized through various surface science techniques. Combining the results obtained it is shown that, at room temperature, metallic Fe nucleates randomly and oxidizes at the interface. A thermal treatment causes Fe migration through the TiO_x layer, forming a mixed oxide and a new hexagonal ultrathin film phase. Finally the pristine TiO_x phase motif is restored, due to the complete diffusion of Fe into the Pt substrate.

Introduction

Ultrathin oxides are well known and widely employed as supports for metal nanoparticles (NPs), so that model surfaces mimicking heterogeneous catalyst can be obtained.[1,2,3] Model catalysts are commonly prepared in ultra high vacuum (UHV) by physical vapour deposition of a metal in an oxygen background, followed by the deposition of metal NPs with a precise control of their amount and dimension. This process allows to obtain single-phase (e.g. SiO_2/Mo(112), Al_2O_3/NiAl(110))[4,5] or multiple-phase (e.g. CrO_x/Pt(111), VO_x/Pd(111), FeO_x/Pt(111))[6,7,8] epitaxial thin oxide films, whose structure and stoichiometry strongly depend on the preparation conditions adopted.

Interestingly, the growth of metal oxides (MO) bilayers on (111) oriented metal single crystals, e.g. VO_x/Rh(111)[9] and FeO_x/Pt(111),8'[10,11] allows to obtain different phases sharing some similarities:

i) a systematic expansion of the lateral lattice parameters with respect to their bulk counterparts

ii) the presence of a nanoscale Moirè periodicity due to the MO_x/Metal(111) lattice mismatch.

Moreover, both FeO_x and TiO_x ultrathin films are good templates for the growth of metallic Au, leading to ordered collections of NPs showing a good dispersion and size selection.[12,13,14] On the contrary, scanning tunneling microscopy (STM) studies of Pd on FeO/Pt(111) showed a wetting behavior of the metal, because of its strong interaction with the substrate.[15] Temperature programmed desorption (TPD), infrared spectroscopy and X ray photoelectron spectroscopy (XPS) studies of this system revealed that after thermal treatment at 600 K Pd diffuses through FeO, to be encapsulated by an oxide bilayer.[16] A similar behaviour was observed after thermal treatment at 970 K of Pt NPs deposited on a rutile-TiO_2(110) single crystal, i.e. a TiO_x bilayer, showing zig-zag like motif, fully coats the metal NPs.[17] More recently the properties of Pt NPs deposited on Fe_3O_4(111)/Pt(111) thin films were studied, and the metal encapsulation by FeO(111) monolayer after annealing at 800 K demonstrated by STM and TPD.[18] A strong adhesion energy between the metal NPs and the support was found to be at the basis of both the diffusion and encapsulation processes. Similar results were reported for other systems, like Co/VO_x[19] and Rh/TiO_x,[20] validating the general conclusion that strong metal support interaction (SMSI) is a characteristic of most metal NPs supported on reducible oxides.[21,22] By means of SMSI metal NPs having high surface energies (like Pt, Rh, Pd) are encapsulated by a reducible oxide support, characterized by a lower surface energy, thus leading to a more stable system.[23]

In this paper we study the morphology and thermal evolution of Fe NPs deposited on a wetting "wagon wheel" TiO_x ultrathin film, called w'-TiO_x, epitaxially grown on Pt(111).[24] It was shown in previous studies that the deposition of TiO_x phases, where Ti atoms are at the interface with Pt and O atoms form the topmost layer, allows to "passivate" the Pt surface, preventing the formation of a Pt-M alloy, while keeping the hexagonal symmetry and metallic properties comparable to those of the Pt substrate. For instance, it was shown that when Au is grown on TiO_x UT phases the metal NPs grow by exposing the (111) surface because of the orienting effect of the underlying Pt substrate.[14] Similarly, when Fe is evaporated on w'-TiO_x/Pt(111) at room temperature, one expects that Fe NPs grow on the ultrathin film substrate without mixing with Pt, whereas interacting with the outermost oxygen layer. The whole set of data will be compared with similar studies relating to Fe NPs deposited on a UT templating oxide, called

[a] Department of Chemical Sciences, University of Padova, via Marzolo 1, I-35131 Padova, Italy.
[b] i-LAMP & Department of Mathematics and Physics, Catholic University, via dei Musei 41, I-25121 Brescia, Italy.
[c] E-mail: luca.artiglia@unipd.it

Physical Chemistry Chemical Physics Accepted Manuscript

z'-TiO_x.[25,26,27] By adopting surface science structural and spectroscopic techniques, such as XPS, TPD, low energy electron diffraction (LEED) and STM, our aim is to show that the structure of the UT film as well as its stoichiometry, entail a change in the thermal evolution of the model catalyst.

Results and discussion

Results

The structure of w'-TiO_x (x=1.2) has been discussed in detail previously:[24,28] it is a double layer of Ti and O atoms with a (7 × 7)-R21.8° commensurate superstructure and forms a flat and continuous film, wetting the Pt(111) surface (see Fig. 1a). STM images (see ref. 24 and Fig. 1a) show a hexagonal unit cell with a unit vector of 19.4 Å, rotated by 21° with respect to the direction of the Pt substrate.

The as-obtained w'-TiO_x UT film is displayed in Figure 1a, whereas Figure 1b refers to the same surface after the deposition of 0.5 MLE of Fe. The wagon wheel motif is not observed after the deposition of the metal, in agreement with the results obtained for the same Fe coverage on the z'-TiOx film.[25] As shown in Figure 2a, Fe NPs have an average diameter of less than 2 nm and an average apparent height of 6±2 Å (Figure 2b). In Figure 1b it is hard to recognize any ordered nucleation pattern, due to the strong affinity and blocked diffusion of the Fe NPs on the oxide support, because of the interaction with the oxygen topmost layer. The lack of order demonstrates that no preferential nucleation sites are present on the w'-TiO_x, in contrast to the z'-TiO_x case.[25,26] Figure 2b shows that, for annealing temperatures as high as 500 K, Fe NPs deposited on the w'-TiO_x have a more pronounced 3D-like morphology, as shown by their sharper average height values, whereas at higher temperatures they assume a 2D-like shape.

XPS data of the Fe/w'-TiO_x/Pt(111) (Ti 2p and Fe 2p core levels), acquired at increasing temperature, are reported in Fig. 3a,c. The Ti 2p signal of the clean UT film (Fig. 1a) shows a broad doublet, the $2p_{3/2}$ peak being centred at about 456.8 eV. A high binding energy (BE) shoulder at about 459.0 eV is detected and can be attributed to stoichiometric TiO_2 clusters that nucleate randomly on the sample surface during the preparation procedure.[13,28] The deposition of 0.5 ML of Fe causes two main effects: a small negative shift of the peak centroid and the reduction in intensity of the high BE shoulder. Both of them can be ascribed to the strong interaction of Fe with the TiO_x oxygen topmost layer, which causes a local reduction of both the TiO_2 clusters and TiO_x film. A change in the morphology of the system does not take place below 500 K, as shown in Fig.1c, i.e. the average height of the Fe NP remains the same as the one measured at RT (Fig. 2b).

A further thermal treatment of the sample causes a positive BE shift of the Ti 2p peak (i.e. after heating at 510 K the Ti 2p peaks maxima are aligned with those of the clean film), whereas a high BE shoulder (ca. 459.0 eV) reappears in the 510-810 K range. Figure 3b shows the Ti 2p difference spectra in the 460-810 K range. A positive peak centred at about 459.0 eV (marked as Ti^{4+}) grows between 510 and 660 K, then decreases. A negative area, whose maximum is found at 456.8 eV, gradually increases above 510 K.

Figure 1d shows a strong modification of the film morphology above 600 K, so that the NPs shape becomes 2D-like, with an average height of 4.5±0.3 Å (Fig. 2b). In the high resolution STM image of Fig. 1e, the motif of an hexagonal wagon-wheel-like ultrathin TiO_x film, compatible with the h-TiO_x phase observed during the Fe (0.5 ML)/z'-TiO_x/Pt(111) system thermal treatment, is observed on top of the islands.[27] This indicates that a diffusion of Fe through the reduced oxide film has occurred. After heating at 810 K, STM shows larger 2D-like islands (Fig 1f), whereas their average electronic height remains around 4.4±0.3 Å (Fig.2b).

A further and dramatic evolution of the film morphology is observed after annealing at 910 K (Fig. 1g-h), i.e. the NPs density decreases, and their average height settles to 2.4±0.1 Å (fig. 2b). Moreover, the wagon-wheel-like motif typical of the w'-TiO_x ultrathin film is observed again. The reduced islands apparent height suggests either a diffusion of Fe into the Pt bulk, or the presence of $PtFe_x$ islands covered by the ultrathin TiO_x film. After a thermal treatment at 960 K, the STM images do not show the presence of Fe islands, either on top or below the TiO_x film (Fig. 1i).

The Fe 2p XPS signal, acquired after deposition at RT, can be associated to the presence of metallic iron (Fe $2p_{3/2}$ peak centroid at about 707.8 eV). Its broad shape can be related both to final state effects, due to the NPs size distribution, and to the presence of oxidized Fe sites, formed because of the strong interaction of metallic Fe with the oxygen topmost layer of the TiO_x film.[29] The thermal treatment causes a positive BE shift and a decrease of the peaks intensity, as shown by the Fe 2p difference spectra (Fig. 3d). The difference spectra display a negative area centred at about 707.1 eV, associated to metallic Fe, whose intensity decreases in the 510-810 K temperature range. Simultaneously, a broad positive peak increases at higher BEs, whose position can be associated to Fe^{2+} (709.3 eV) and Fe^{3+} (711.0 eV).[30] At 810 K a peak centred at about 725.7 eV, assigned to Pt 4s, becomes predominant and grows until 960 K.

TPD spectra (Fig. 3), acquired using CO as a probe molecule, are extremely useful to check the chemisorption sites and chemical properties of the sample surface. The desorption spectrum, acquired on the as prepared Fe(0.5 ML)/w'-TiO_x/Pt(111) sample, displays a broad peak centred at about 360 K, attributable to metal Fe sites,[31] whereas less intense peaks, due to both Fe^{2+} and Fe^{3+} sites, are found in the 140-180 K range.[32,33] After the first thermal treatment (460 K), the 360 K peak is almost totally extinguished, whereas the Fe^{n+} peaks become predominant. According to the literature, desorption peaks at 140 and 155 K are due to Fe^{2+}, whereas the one at 170 K to Fe^{3+}.[32,33] The CO desorption profile evolves as function of the temperature, i.e. the peak at 170 K (desorption from Fe^{3+} sites) decreases and vanishes between 560 and 610 K, whereas the peaks associated to Fe^{2+} become less intense, but are still present after the last annealing at 960 K, meaning that a few Fe^{2+} adsorption sites are available on the sample surface. Above 910 K, a broad peak at about 370 K starts to grow, and after thermal treatment at 960 K its position shifts to 390 K. Considering that no CO desorption peaks were observed immediately after the w'-TiO_x film deposition, demonstrating that the Pt(111) substrate was fully covered, the 370 K peak can be

Physical Chemistry Chemical Physics Accepted Manuscript

This journal is © The Royal Society of Chemistry 20xx

associated to CO desorption from patches of a $PtTi_x$ alloy, formed by partial thermal reduction of the TiO_x UT film.[34] On the other hand, the 390 K peak (see Fig. 4b for the zoom in of the RT, 910 and 960 K TPD spectra) can be associated to the desorption of CO from uncovered Pt islands, confirming the diffusion of Fe into the support. A similar trend was reported on Fe/z'-TiO_x in the 760-810 K temperature range.[25]

LEED images (Figure 5) show that after Fe deposition the diffraction spots of the w'-TiO_x phase are strongly attenuated, whereas after the thermal treatments (up to 960 K) the pattern changes. By comparison with the data reported in the literature,[28] it is possible to conclude that the observed LEED pattern is formed by the superimposition of the w'- and the z'-TiO_x diffraction spots. The presence of the z' phase indicates that the thermal treatment causes a partial diffusion of Ti inside the Pt(111) (the z'-TiO_x forms at coverages lower than the MLE).

Discussion

To discuss the data it is worth recalling the Fe/z'-TiO_x/Pt(111) system behaviour observed in the same conditions. As already mentioned in the introduction, the morphology and thermal evolution of Fe NPs deposited on the z'-TiO_x UT film have been analyzed in detail in other studies.[25,26,27] Differently from the w'-TiO_x UT film, the z'-TiO_x, which is obtained at lower coverages, has a $TiO_{1.25}$ stoichiometry and consists in stripes with a zig-zag like motif (due to the different coordination of Ti atoms) separated by dark rows (called troughs).[35] Ordered arrays of defects (titanium vacancies), where the Pt substrate is uncovered, called picoholes, are detected along the troughs by STM.[28,36] Such defects act as preferential nucleation sites for metal NPs[13,36,37] and, also in the case of Fe NPs, have a "templating" effect.[26] The analysis of the Fe/z'-TiO_x/Pt(111) thermal evolution revealed that, because of the strong tendency of Fe to alloy with Pt,[38] Fe diffuses into the Pt(111) substrate by migrating through the TiO_x UT film.[25,26,27] The migration starts already at temperatures close to RT (ca. 400 K) and continues until 700 K. During this process a mixed FeO_x/TiO_x oxide is formed and the film rearranges into a new, more reduced ($TiO_{1.14}$), hexagonal phase (called h-TiO_x),[27] whereas at higher temperatures (in the 800-900 K range) the pristine z' phase is restored.

We want to start our discussion considering the XPS, TPD and STM data collected immediately after Fe deposition. At RT, a shift of about 0.5 eV in the Ti 2p spectrum (Fig. 3a) is measured. Moreover the Fe 2p peaks (Fig. 3c) have a broad shape, in agreement with the presence of more than one oxidation state, as already observed for Fe/z'-TiO_x. The former effect may be explained by a local reduction of TiO_x taking place after Fe deposition, due to the strong affinity between the Fe metallic NPs and the w'-TiO_x film oxygen topmost layer. On the other hand, the Fe $2p_{3/2}$ peak maximum is found at 707.8 eV, a BE value typical of metallic Fe. Its broad shape can be associated either to final state effects connected to the NPs dimensions or to the presence of Fe^{n+} sites. The CO desorption profile (Fig. 4a,b) shows, as expected, a predominant metallic component (peak centred at 360 K), whereas the peaks related to Fe^{n+} sites are barely visible (140-170 K temperature range). Comparing our TPD data with those referring to CO desorption from a Fe single crystal surface,[31] a negative shift of about 50 K is noticed. This can be explained by a charge transfer from Fe to the oxygen terminated TiO_x bilayer, which affects the π-back donation from the Fe d orbitals to the adsorbed CO π* orbitals. Therefore, Fe NPs supported on w'-TiO_x are less electron rich, so that a lower amount of energy is required for the desorption of CO. Considering both TPD and XPS results acquired after Fe deposition, it is demonstrated that the Fe 2p position and broad shape are mainly due to final state effects, whereas Fe^{n+} sites probably form at the NPs edges. This is in contrast with the results collected on the Fe/z'-TiO_x,[25,26] where CO desorption from both metallic and Fe^{n+} sites was observed already at RT. Such a difference can be explained by taking into consideration the nucleation and growth modes of the Fe NPs on the two examined TiO_x UT films. The ordered arrays of defects (picoholes) on the z'-TiO_x act as preferential nucleation sites, allowing a strong interaction between Fe and TiO_x along the troughs. Furthermore, picoholes act as preferential Fe diffusion paths into the Pt bulk. When Fe is deposited on the w'-TiO_x the NPs nucleate and grow randomly (as shown in Fig. 1b), i.e. no preferential decoration of step edges, which are areas of the support where a large number of undercoordinated sites is present, is observed. The only way for Fe to diffuse toward the Pt substrate is to "destroy" locally the UT oxide film. In a previous STM study of Au NPs grown on TiO_x/Pt(111) it was demonstrated that the metal/support interaction affects enormously the NPs morphology.[39] Au NPs deposited on a reduced TiO_x film showed low average diameters (between 1.5 and 2.0 nm) and apparent height (around 0.5 nm), very similar to the morphology of Fe NPs on w'-TiO_x/Pt(111) observed in this work (Fig. 1b and Fig. 2). The energy barrier for Au NPs diffusion on a reduced TiO_x film was computed (Density functional theory) to be around 2.4 eV. On the contrary, Au NPs deposited on stoichiometric TiO_2 islands showed three-dimensional growth (apparent height of 1.5 nm) and larger NPs size (average diameters around 6.0 nm). In that case the calculated energy barrier for NPs diffusion was below 0.06 eV.[39] Based on these results we can hypothesize a strong interaction between Fe and the TiO_x film limited to the interface, leading to a local Fe→O charge transfer and thus Ti reduction.

After thermal treatment at 460 K a new transformation takes place, because the CO desorption profile does not show any metallic Fe sites (the 360 K peak is quenched), whereas 3 intense and well resolved peaks, corresponding to the Fe^{n+} sites, develop at lower temperature (ca. 140, 155 and 170 K). A mild thermal treatment (460 K) is enough to promote the almost complete conversion of metallic Fe into FeO_x, as also demonstrated by a shift of the Fe 2p XPS peak to higher BEs (Fig. 3c), although this chemical modification does not imply an evident morphological change of the system, as shown both by STM images (Fig. 1a and b) and line profile (constancy of the NPs apparent height (Fig. 2b)).

A further increase in the temperature promotes Fe diffusion through the w'-TiO_x film, together with a re-ordering of the system, as shown in Fig. 1d-e (610 K), where more regularly shaped and faceted NPs are displayed. Starting from 510 K the Fe 2p peaks gradually decrease in intensity, due to the onset of Fe diffusion through the w'-TiO_x film, and shift to higher BE, due to the higher amount of the Fe^{n+}. The Fe 2p difference spectra (Fig. 2d) show that the metallic component (707.1 eV) is associated with a negative

Physical Chemistry Chemical Physics Accepted Manuscript

area due to metallic Fe diffusion, whereas Fe^{2+} and Fe^{3+} (at 709.3 and 711.0 eV, respectively) originate a positive area.

In the same temperature range (510-810 K), a component centred at about 459.0 eV, assigned to Ti^{4+}, starts to develop in the Ti 2p spectrum. This is also shown by the Ti 2p difference spectra in Fig. 3b, i.e. positive area at 459.0 eV reaches the highest intensity at about 660 K and then decreases. The negative area centred around 456.8 eV indicates that part of the TiO_x film oxidizes already at low temperatures. Moreover, its monotonic increase (in absolute value) suggests that the TiO_x film starts to decompose at higher temperatures, by diffusion of Ti into the Pt substrate. This explains why the peaks area, after annealing to 810 K, is lower than the one acquired at RT. Besides a certain amount of Ti loss it is important to notice, as already seen for Fe/z'-TiO_x,[25,26,27] that Fe diffuses through the TiO_x layer by forming a FeO_x/TiO_x mixed oxide. This explains why simultaneous oxidation is observed in the Ti and Fe 2p XPS signals in the 510-810 K temperature range.

The high resolution STM image acquired after annealing at 610 K (Fig. 1e) show triangular-hexagonal patches, which can be associated to the formation of a new hexagonal (h-TiO_x) phase structure, already found during the thermal treatment of the Fe/z'-TiO_x.[25,27] Since in the case of the Fe/z'-TiO_x system the Fe-mediated phase transition (z'-TiO_x→h-TiO_x) was observed already at 410 K, it was concluded (based on DFT calculations) that the reaction:[27]

$$z'\text{-}TiO_{1.25}/Pt + 0.15\ Fe \rightarrow 0.70\ h\text{-}TiO_{1.14}/Pt + 0.15\ FeTiO_3 + 0.15\ Ti$$

was favoured by the ordered arrays of defects of the z'-TiO_x phase. On the contrary, after Fe is deposited on the flat, oxygen terminated w'-TiO_x layer, a higher activation energy is required for Fe to react with the TiO_x film and diffuse through it. Therefore, a further parameter affecting the Fe-TiO_x interaction is its stoichiometry, i.e. the Fe diffusion process requires more energy to occur because the w'-TiO_x (x=1.2) is more reduced than the z'-TiO_x (x=1.25) UT film.

The simultaneous intensity decrease of the 459.0 eV component (Fig. 3a,b), of the Fe 2p peaks area (Fig. 3c,d) and of the CO desorption peaks associated to Fe^{n+} sites (Fig. 3), observed in the 660 – 810 K temperature range, agrees well with Fe reaction with the TiO_x film. A possible LEED pattern for $FeTiO_3$ (ilmenite) growing on Pt(111) has been simulated (not shown). A commensurate LEED pattern can be obtained assuming a -1.87% strain with respect to the Pt support (2a decreases from 10.18 to 9.99 Å). STM images of this superstrucure should show islands characterized by an hexagonal symmetry. Although we never observed any LEED pattern corresponding or similar to that of ilmenite in the 610-800 K temperature range, probably because of the small NPs size, the triangular shaped islands displayed in Fig. 1e are in agreement with the simulation.

After heating at 910 K, nearly all the Fe 2p XPS signal disappears, the Ti 2p recovers its original position and shape and HR-STM images (Fig 1g-h) show that the original wagon-wheel motif is mostly recovered. Therefore, we can hypothesize that the residual FeO_x/TiO_x mixed oxide islands decompose, leading to further diffusion of Fe into the Pt substrate and recover of the original $TiO_{1.2}$ stoichiometry by re-oxidation of the h-$TiO_{1.14}$. In this case a possible (reversible) reaction would be:

$$w'\text{-}TiO_{1.2}/Pt + 0.10Fe \rightarrow 0.80\ h\text{-}TiO_{1.14} + 0.10\ FeTiO_3 + 0.10\ Ti$$

Interestingly, the LEED image (Fig. 5), obtained after thermal treatment at the highest temperature (960 K) shows the w'-TiO_x pattern together with that of the z'-TiO_x. This proves the small, temperature mediated, Ti diffusion into the Pt substrate, as also demonstrated by the decrease in the Ti 2p signal overall area. Indeed, the TiO_x/Pt(111) phase diagram shows that the z'-TiO_x grows at lower Ti loading. Also the TPD data confirm this hypothesis: the peaks at 370 and 390 K, detected in the 910-960 K annealing range (Fig. 4b) are typical of CO desorption from a $PtTi_x$ alloy and Pt, respectively. $PtTi_x$ patches form as a consequence of local thermal-mediated reduction of the TiOx film, whereas the diffusion of Ti into the bulk leads to the formation of uncovered Pt islands.

Experimental

Materials and methods

Prior to TiO_x deposition the Pt(111) single crystal was cleaned through Ar^+ sputtering cycles and annealed at 970 K in UHV until no C 1s signal was detectable by XPS. The (1x1) surface reconstruction was checked by LEED. The w'-TiO_x UT film was grown by deposition of about 1 monolayer equivalent (MLE) of metal Ti (electron beam evaporation) in a 1.0 x 10^{-7} mbar oxygen ambient at room temperature (RT), followed by thermal treatment in UHV at 950 K. The MLE of TiO_x was determined based on the TiOx/Pt(111) phase diagram, which correlates the UT film thickness to the specific phase obtained.[28] 0.5 MLE of Fe were deposited at RT in UHV with an electron beam evaporator. The Fe MLE was calibrated according to the XPS intensity ratio between Fe and Pt. The thermal evolution was monitored by thermalisation (2 min) of the Fe/w'-TiO_x/Pt(111) system at increasing temperatures in the RT-960 K range.

XPS data were recorded using a double anode soft x ray source (Omicron, Al Kα photon, 1486.6 eV) and a single channeltron VG CLAM 2 photoelectron analyzer. The TPD data were collected with a Hiden quadrupole mass spectrometer (QMS) covered by a quartz shield. A 6 mm hole, located close to the ionization cage, was placed at ca. 2 mm from the sample, allowing the desorption product analysis to focus on the model catalyst surface. The sample was mounted on a UHV manipulator with 4 degrees of freedom, spot-welded to 2 Ta wires and the temperature was read by a type K thermocouple. All the desorption experiments were performed after cooling down the sample to 120 K with liquid nitrogen, dosing 1.0 L of CO and heating with a linear (2.0 K/s) temperature ramp to 470 K. A background spectrum, corresponding to CO desorption from the clean w'-TiO_x UT film, was subtracted to each spectrum acquired on the Fe/w'-TiO_x system, to focus the analysis on the Fe NPs.

The STM images were acquired in constant current mode at RT, using an Omicron multiscan system, with tip to sample bias

Physical Chemistry Chemical Physics Accepted Manuscript

This journal is © The Royal Society of Chemistry 20xx

ranging from +0.7 V to +2 V and tunneling current ranging from 0.2 nA to 2 nA. A Pt/Ir tip was prepared by electrochemical etching in saturated $CaCl_2$ aqueous solution and subsequently cleaned in UHV by electron bombardment.

Conclusions

In this study we have shown that a nanostructured model system, obtained depositing Fe NPs on a fully wetting TiO_x UT film epitaxially grown on Pt(111) undergoes relevant morphological and chemical transformations due to the metal/TiO_x interaction and to its thermal treatment up to 960 K. At RT Fe interacts strongly with the reduced TiO_x layer, binding to the oxygen topmost layer to form FeO_x at the interface. These Fe NPs are less electron rich than bulk Fe or Fe NPs supported on clean metal surfaces, as shown by CO-TPD data. This behavior suggests that the formation of a w'-TiO_x/Pt structure is a way to modulate the reactivity of easily oxidizable metals like Fe.

In the 560-860 K Fe diffuses through the TiO_x UT film toward the Pt substrate. During this process, a FeO_x/TiO_x mixed oxide is formed, and the pristine TiOx UT film morphology is almost totally lost. A w'-$TiO_x \rightarrow$h-TiO_x phase transformation is observed, due to a partial reduction of the pristine film. The Fe diffusion process ends between 910 and 960 K, i.e. FeO_x gives its oxygen back to the TiO_x film, allowing the reappearance of the w' phase motif. The comparison with previous studies, focusing on the growth and thermal evolution of Fe NPs on another TiO_x film (z'-TiO_x) demonstrates that on a fully wetting layer like w'-TiO_x, where no preferential nucleation sites are found, Fe NPs grow randomly (no templating effect seen in the case of z'-TiO_x). Moreover, the onset of Fe diffusion toward Pt is observed at higher temperatures, demonstrating that defects (picoholes in the case of the z'-phase) promote the reaction.

A study of the deposition of Co on VO_x/Rh(111) showed that the metal diffuses underneath the oxide film already at RT.[19] The authors concluded that the balance of surface free energies drives the system towards the encapsulation of the metal overlayer by the VO_x. The metal diffusion is favored because surface free energies of oxides are generally lower than those of metals. By studying the interaction of Fe with two TiO_x UT films we have demonstrated that the surface oxide stoichiometry and its defectivity are important parameters to be considered as well.

Ultrathin oxide films on metals/metals NPs are known to be good catalysts (the so-called monolayer catalysts),[40] particularly with respect to the oxidation of CO.[41] Recent results reveal that weakly bound oxygen species are directly correlated to the enhanced activity.[42] Theoretical calculations predicted a polaronic distorsion effect leading to the stabilization of surface $O^{2\bullet-}$ radicals on very thin oxide films (e.g. MgO (001) on Mo(001)).[43] As an example, in the case of FeO_x/Pt(111), O_2 molecules from the gas phase interact with the oxide layer, pulling a Fe atom from the metal/oxide interface to the outermost layer and forming transient O^{2-} species. Our TiO_x/Fe system could in principle be compared to other monolayer catalysts, although we have to take into consideration that once Fe diffuses through the TiO_x film it goes in contact with the Pt(111) surface. It is reported in the literature that Fe has a strong tendency to alloy with Pt,[44] thus the catalytic tests on our system should be limited to a narrow temperature range (between RT and 500 K).

Acknowledgements

This work has been funded by the Italian Ministry of Instruction, University and Research (MIUR) through the FIRB Project RBAP115AYN "Oxides at the nanoscale: multifunctionality and applications".

Physical Chemistry Chemical Physics Accepted Manuscript

Journal Name

ARTICLE

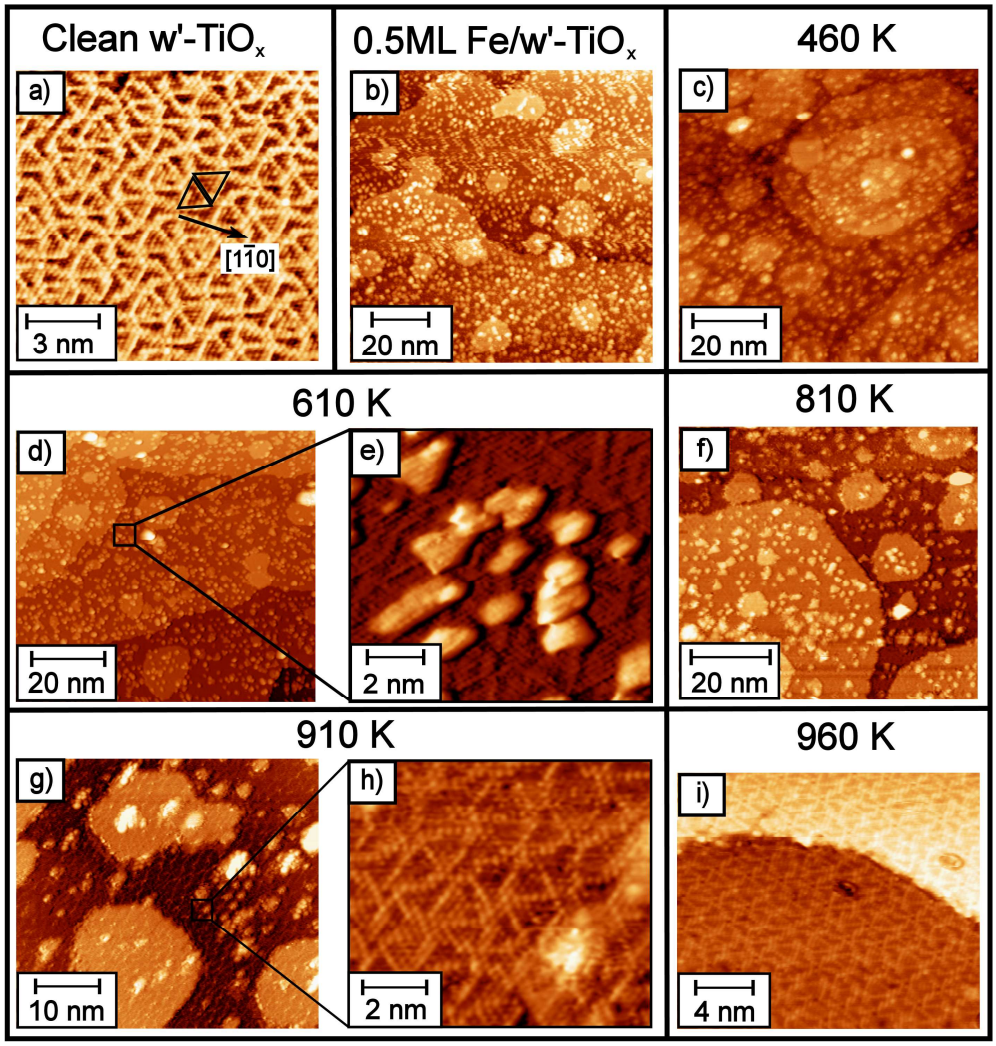

Fig. 1 a) (V= +0.74 V; I=1.24 nA) Atomic resolution frame of pristine w'-TiOx/Pt(111) film. b) (V= +2.0 V; I=0.2 nA) Film morphology after deposition of 0.5 ML of Fe. c) (V= +2.0 V; I=0.2 nA) Film morphology after 460 K annealing in UHV. d) (V= +2.0 V ; I=0.2 nA) and e)(V= +1.14 V; I= 2.04 nA) Film morphology after 610 K annealing step. f) (V= +1.8 V; I= 0.2 nA) Film morphology after 810 K annealing step. g) (V= +2.0 V; I= 0.21 nA) and h) (V= +1.08 V; I= 1.43 nA) Film morphology after 910 K annealing step. i) (V=+1.4 V; I=0.51 nA) High resolution frame of the film appearance after last annealing step at 960K, no more Fe NPs are observed.

Physical Chemistry Chemical Physics Accepted Manuscript

Please do not adjust margins

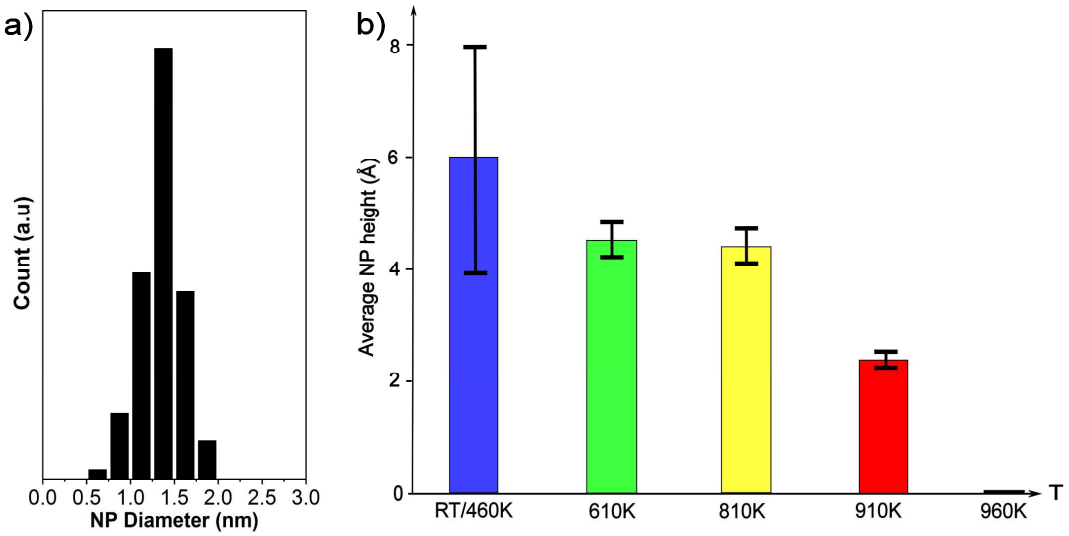

Fig. 2 a) Size distribution of NPs formed upon deposition at RT of 0.5 ML of Fe on w'-TiOx film, extracted from fig. 1b. b) Evolution of the apparent height of the Fe NPs on w'-TiOx film versus sequential annealing at rising temperatures. After thermal treatment at 960K no more Fe NPs are observed on the surface. Error bars related to the statistical variance of the measured apparent height of the Fe NPs are also reported.

Physical Chemistry Chemical Physics Accepted Manuscript

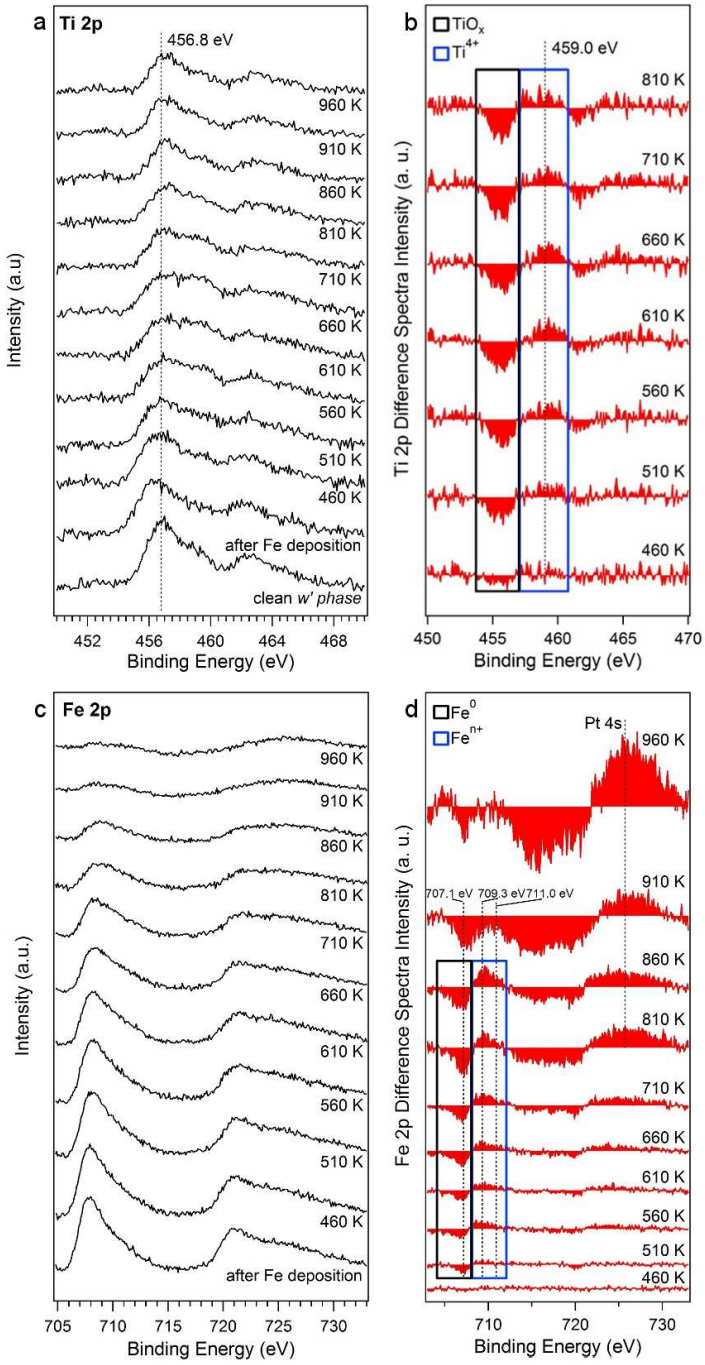

Fig. 3 XPS signals collected on a Fe(0.5 ML)/w'-TiOx/Pt(111) in the RT-960 K temperature range: a) Ti 2p, b) Ti 2p difference spectra, c) Fe 2p, d) Fe 2p difference spectra.

Physical Chemistry Chemical Physics Accepted Manuscript

This journal is © The Royal Society of Chemistry 20xx

Please do not adjust margins

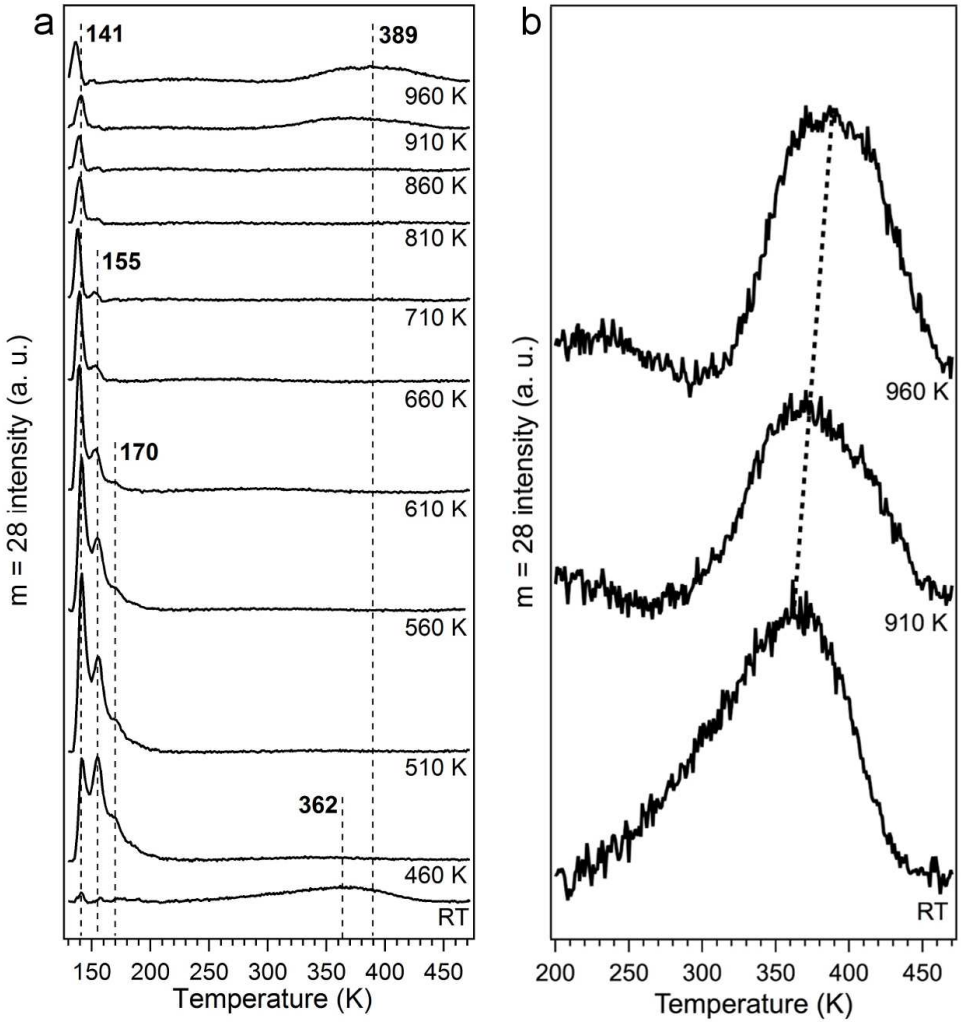

Fig. 4 a) TPD spectra collected on a Fe(0.5 ML)/w'-TiOx/Pt(111) at RT and after thermal treatment (2 minutes) in the RT-960 K temperature range, b) zoom in of the RT, 910 and 960 K spectra.

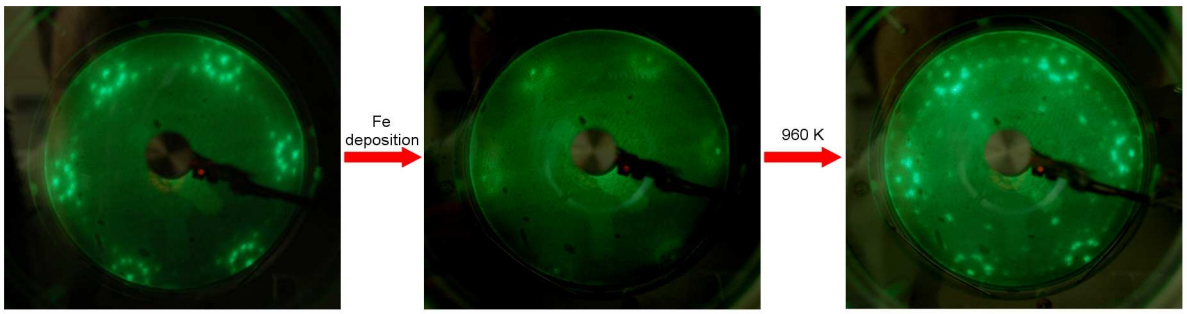

Fig. 5 LEED patterns (imaged at RT, 55.0 eV) of the clean w'-TiOx (left), the Fe(0.5 ML)/w'-TiOx/Pt(111) (center) and Fe(0.5 ML)/w'-TiOx/Pt(111) annealed at 960 K for 2 minutes (right).

Physical Chemistry Chemical Physics Accepted Manuscript

Journal Name

ARTICLE

Notes and references

1 M. Bäumer and H.-J. Freund, *Progr. Surf. Sci.*, 1999, **61,** 127.
2 Q. Fu and T. Wagner, *Surf. Sci. Rep.*, 2007, **62**, 431.
3 R. J. White, R. Luque, V. L. Budarin, J. H. Clarka and D. J. Macquarrie, *Chem. Soc. Rev.*, 2009, **38**, 481.
4 T. Schroeder, M. Adelt. B. Richter, M. Naschitzki, M. Baumer and H. J. Freund, *Surf. Rev. Lett.*, 2000, **7**, 7.
5 T. Bertrams, A. Brodde and H. Neddermeyer, *J. Vac. Sci. Technol. B*, 1994, **12**, 2122.
6 P. S. Robbert, H. Geislerl, C. A. Ventrice Jr., J. van Ek, S. Chaturvedi, J. A. Rodriguez, M. Kuhn and U. Diebold, *J. Vac. Sci. Technol A*, 1998, 16, 990.
7 S. Surnev, L. Vitali, M. G. Ramsey, F. P. Netzer, G. Kresse and J. Hafner, *Phys. Rev. B*, 2000, **61**, 13945.
8 H. C. Galloway, J. J. Benítez and M. Salmeron, *J. Vac. Sci. Technol. A*, 1994, **12**, 2302.
9 J. Schoiswohl, S. Surnev, M. Sock, S. Eck, M.G. Ramsey, F.P. Netzer and G. Kresse, *Phys. Rev. B*, 2005, **71**, 165437.
10 M. Ritter, W. Ranke and W. Weiss, *Phys. Rev. B*, 1998, **57**, 7240.
11 Y.I. Kim, C. Westphal, R.X. Ynzunza, H.C. Galloway, M. Salmeron, M.A. van Hove and C.S. Fadley, *Phys. Rev. B*, 2000, **55**, R13448.
12 N. Nilius, E.D.L. Rienks, H.P. Rust and H.-J. Freund, *Phys. Rev. Lett.*, 2005, **95**, 066101.
13 F. Sedona, S. Agnoli, M. Fanetti, I. Kholmanov, E. Cavaliere, L. Gavioli and G. Granozzi, *J. Phys. Chem. C*, 2007, **111**, 8024.
14 G. A. Rizzi, F. Sedona, L. Artiglia, S. Agnoli, G. Barcaro, A. Fortunelli, E. Cavaliere, L. Gavioli and G. Granozzi, *Phys. Chem. Chem. Phys.*, 2009, **11**, 2177.
15 Sh.K. Shaikhutdinov, R. Meyer, D. Lahav, M. Bäumer, T. Klüner and H.-J. Freund, *Phys. Rev. Lett.*, 2003, **91**, 076102.
16 R. Meyer, D. Lahav, T. Schalow, M. Laurin, B. Brandt, S. Schauermann, S. Guimond, T. Klüner, H. Kuhlenbeck, J. Libuda, Sh. Shaikhutdinov and H.-J. Freund, *Surf. Sci.*, 2005, **586**, 174.
17 O. Dulub, W. Hebenstreit and U. Diebold, *Phys. Rev. Lett.*, 2000, **84**, 3646.
18 Z.-H. Qin, M. Lewandowski, Y.-N. Sun, S. Shaikhutdinov and H.-J. Freund, *J. Phys. Chem. C*, 2008, **112**, 10209.
19 G. Parteder, F. Allegretti, S. Surnev and F. P. Netzer, *Surf. Sci.*, 2008, **602**, 2666.
20 A. Berkó, R. Gubó, L. Óvári, L. Bugyi, I. Szenti and Z. Kónya, *Langmuir*, 2013, **29**, 15868.
21 S. J. Tauster, S. C. Fung and R. L. Garten, *J. Amer. Chem. Soc.*, 1978, **100**, 170.
22 S. J. Tauster, *Acc. Chem. Res.*, 1987, **20,** 389.
23 H. Knozinger and E. Taglauer, *In Handbook of Heterogeneous Catalysis*, Eds. VCH: Weinheim, Germany, 1997; p. 216
24 F. Sedona, S. Agnoli and G. Granozzi, *J. Phys. Chem. B*, 2006, **110**, 15359.
25 L. Artiglia, E. Cavaliere, G. A. Rizzi, L. Gavioli and G. Granozzi, *J. Phys. Chem. Lett.*, 2010, **1**, 1660.
26 L. Artiglia, E. Cavaliere, A. Vascon, F. Bondino, G. A. Rizzi, L. Gavioli and G. Granozzi, *J. Phys. Chem. C*, 2011, **115**, 15812.
27 E. Cavaliere, L. Artiglia, G. Barcaro, G. A. Rizzi, F. Bondino, A. Fortunelli, L. Gavioli and G. Granozzi, *Phys. Chem. Chem. Phys.*, 2011, **12**, 17171.
28 F. Sedona, G. A. Rizzi, S. Agnoli, F. X. Llabrés i Xamena, A. Papageorgiou, D. Ostermann, M. Sambi, P. Finetti, K. Schierbaum and G. Granozzi, *J. Phys. Chem. B*, 2005, **109**, 24411.
29 G. Barcaro and A. Fortunelli, *J. Phys. Chem. A*, 2009, **113**, 14860.
30 G. Bhargava, I. Gouzman, C. M. Chun, T. A. Ramanarayanan and S. L. Bernasek, *Appl. Surf. Sci.*, 2007, **253**, 4322.
31 S. D. Cameron and D. J. Dwyer, *Langmuir*, 1988, **4**, 282.
32 C. Lemire, R. Meyer, V. E. Henrich, S. Shaikhutdinov and H. J. Freund, *Surf. Sci.*, 2004, **572**, 103.
33 Y. N. Sun, Z. H. Qin, M. Lewandowski, S. Shaikhutdinov and H. J. Freund, *Surf. Sci.*, 2009, **603**, 3099.
34 S. Le Moal, M. Moors, J. M. Essen, C. Becker and K. Wandelt, *Surf. Sci.*, 2010, **604**, 1637.
35 F. Sedona, G. Granozzi, G. Barcaro and A. Fortunelli, *Phys. Rev. B*, 2008, **77**, 115417.
36 E. Cavaliere, I. Kholmanov, L. Gavioli, F. Sedona, S. Agnoli, G. Granozzi, G. Barcaro and A. Fortunelli, *Phys. Chem. Chem. Phys.*, 2009, **11**, 11305.
37 L. Gavioli, E. Cavaliere, S. Agnoli, G. Barcaro, A. Fortunelli and G. Granozzi, *Prog. Surf. Sci.*, 2011, **86**, 59.
38 D. I. Jerdev and B. E. Koel, *Surf. Sci.*, 2002, **513**, L391.
39 F. Sedona, M. Sambi, L. Artiglia, G. A. Rizzi, A. Vittadini, A. Fortunelli and G. Granozzi, *J. Phys. Chem. C,* 2008, **112**, 3187.
40 Y.-N. Sun, L. Giordano, J. Goniakowski, M. Lewandowski, Z.-H. Qin, C. Noguera, S. Shaikhutdinov, G. Pacchioni and H.-J. Freund, *Angew. Chem. Int. Ed.,* 2010, **49**, 4418.
41 Y.-N. Sun, Z.-H. Qin, M. Lewandowski, E. Carrasco, M. Sterrer, S. Shaikhutdinov and H.-J. Freund, *J. Catal.*, 2009, **266**, 359.
42 Y. Martynova, S. Shaikhutdinov and H.-J. Freund, *ChemCatChem*, 2013, **5**, 2162.
43 A. Gonchar, T. Risse, H.-J. Freund, L. Giordano, C. Di Valentin and G. Pacchioni, *Angew. Chem. Int. Ed.*, 2011, **50**, 2635.
44 D. I. Jerdev and B. E. Koel, *Surf. Sci.*, 2002, **513**, L391.

Physical Chemistry Chemical Physics Accepted Manuscript